Supporting Information: Image-charge effects on ion adsorption near aqueous interfaces

Chang Yun Son[a,b,c] **and Zhen-Gang Wang**[a,1]

[a]Division of Chemistry and Chemical Engineering, California Institute of Technology, Pasadena, CA 91125, USA; [b]Department of Chemistry, Pohang University of Science and Technology, Pohang, 37673, South Korea; [c]Division of Advanced Materials Science, Pohang University of Science and Technology, Pohang, 37673, South Korea

Edited by Monica Olvera de la Cruz, Northwestern University, Evanston, IL, and approved March 16, 2021 (received for review October 1, 2020)

Contribution of ICI induced by two parallel conducting plates to the total electrostatic energy in model systems

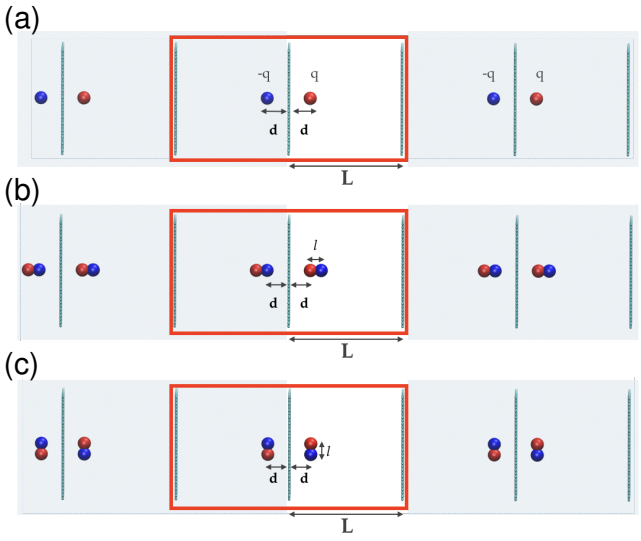

Fig. S1. Schematic drawings of the infinite series of ICPs generated by (a) a single ion, (b) a single dipole perpendicular to the conducting surface, and (c) a single dipole parallel to the conducting surface. Red and blue spheres represent ions and ICPs with positive and negative charge, respectively. The red rectangular box shows the periodic unit cell of the infinite series of ICPs. The contribution of ICI to the total electrostatic energy (E_{ICI}) is exactly half of the interaction energies between the real particles (RPs) in the central primary cell and all of the ICPs in the shaded area.[1]

Single ion and symmetric ion pair. In this section, we compare the contribution of ICI to the total electrostatic energy of the system, which can be calculated by counting exactly half of the sum of electrostatic energies of all possible combinations of real particle-image charge particle (RP-ICP) pairs.[1] The simplest case is a single ion with charge q placed in the primary cell of length L (Fig. S1)(A). Thus this ICI energy of single ion (SI, E_{SI}^{ICI}) can be calculated by,

$$E_{SI}^{ICI}(x) = \frac{q^2}{\epsilon L}\frac{1}{2}\sum_{n=1}^{\infty}\left(\frac{2}{2n} - \frac{1}{2n-2x} - \frac{1}{2(n-1)+2x}\right)$$
$$= \frac{q^2}{\epsilon L}\frac{1}{4}\left(2\gamma + \psi(1-x) + \psi(x)\right) \qquad [S1]$$

where $x = d/L < .5$, $\gamma = 0.5772...$ is the Euler-Mascheroni constant, and $\psi(x)$ is digamma function defined as the logarithmic derivative of the gamma function $\psi(x) = \Gamma'(x)/\Gamma(x)$. As discussed in the main text, Eq. 1 in the main text calculates the ICI energy contribution for a symmetric ion pair (IP_sym, $E_{IP_{sym}}^{ICI}$) where the two ions are placed at the same distance from the two surfaces. As plotted in Fig. S2, both E_{SI}^{ICI} (black solid line) and $E_{IP_{sym}}^{ICI}$ (yellow solid line) are always negative and diverges to negative infinity as the ions approach to zero distance from the conducting surfaces. We note that in real systems, the finite size of the ions prevents this singularity. An important difference between the two ICI energy contributions is that while $E_{IP_{sym}}^{ICI}$ converges to zero as the ions approach the center of the primary cell (no charge separation), E_{SI}^{ICI} converges to a finite negative number ($(\gamma+\psi(.5))/2 \approx -0.69$). Also the two functions cross at near $x = 0.2$, such that $E_{IP_{sym}}^{ICI}$ becomes more negative when the ion pairs are near the surface. Note that the total electrostatic energy for the symmetric ion pair, $E_{IP_{sym}} = E_{IP_{sym}}^{ICI} - q^2/\epsilon L(1-2x)$ (yellow dashed line in Fig. S2), has two minimum energy configurations at $x = 0, 0.5$; one where the ions are combined (to a minimum cut-off distance) and another where they touch the surface (to a minimum cut-off distance). The second minimum drives the system to prefer a state with greater charge separation along the z-axis. As a result, the ICI contribution to the electrostatic force acting on the ions is greater for symmetric ion pair than a single ion moving toward the surfaces, which explains why

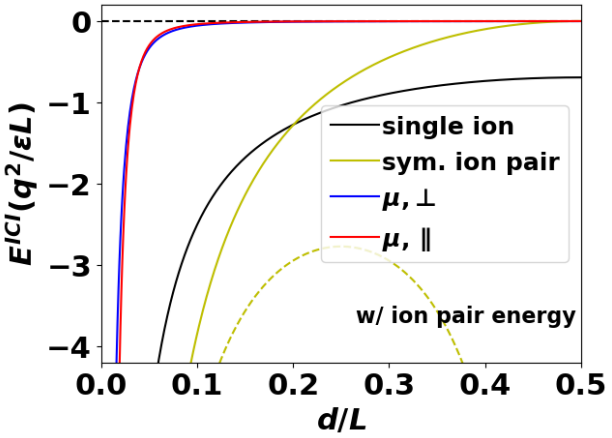

Fig. S2. The ICI contribution to the total electrostatic energy for a single ion (E_{SI}^{ICI}, black) and a symmetric ion pair ($E_{IP_{sym}}^{ICI}$, yellow), as well as a dipole that is either perpendicular ($E_{\mu_\perp}^{ICI}$, blue) or parallel ($E_{\mu_\parallel}^{ICI}$, red) to the conducting surface. All energy contributions are always negative and diverge to negative infinity when the ions touch the conducting surface. $E_{IP_{sym}}^{ICI}$ converges to zero as the ions approach the center of the primary cell (no charge separation). The yellow dashed line shows the total electrostatic energy for the symmetric ion pair, which includes both the $E_{IP_{sym}}^{ICI}$ and the direct Coulomb interaction energy between the ion pair. ICI for the dipole with both orientations converges quickly to zero as d increases, illustrating that dipolar ICIs are much shorter-ranged compared to the ICI induced by single ion or a symmetric ion pair that are separated at the same distance from the opposite surfaces. Two dipole ICI are similar in magnitude except at very short distance from the surface.

the simulations under 1V electric potential difference showed greater ICI effect.

Single dipole with perpendicular or parallel orientation with respect to the conducting surfaces. The ICI effect induced for a single dipole or multi-atomic molecules depend on the orientation of the molecules relative to the conducting surfaces. Here, we compare two extreme cases, namely a dipole that is either perpendicular or parallel to the conducting surfaces as shown in Figs. S1(b,c). The dipole μ is composed of two oppositely charged particles that are separated by distance l, and the positively charged particle is placed at the distance d from the left surface. To calculate the full $E^{ICI}_{\mu_\perp}$, we need to consider contributions from four series of RP-ICP pairs $E^{ICI}_{\alpha\beta}$, where α indicates the positive (+) or negative (-) RP, and β indicates ICPs induced by the (+) or (-) RP. Now the ICI energy contribution to the total electrostatic energy can be calculated by the sum of the contributions from each of the four series of pairs as,

$$E^{ICI}_{\mu_\perp}(x,y) = E^{ICI}_{++_\perp}(x,y) + E^{ICI}_{+-_\perp}(x,y) + E^{ICI}_{-+_\perp}(x,y) + E^{ICI}_{--_\perp}(x,y) \quad [S2]$$

where $y = l/L$ and

$$\begin{aligned} E^{ICI}_{++_\perp}(x,y) &= E^{ICI}_{SI}(x), \\ E^{ICI}_{+-_\perp}(x,y) = E^{ICI}_{-+_\perp}(x,y) &= \frac{q^2}{\epsilon L}\frac{1}{2}\sum_{n=1}^{\infty}\left(-\frac{1}{2n+y} - \frac{1}{2n-y} + \frac{1}{2n-2x-y} + \frac{1}{2(n-1)+2x+y}\right) \\ &= \frac{q^2}{\epsilon L}\frac{1}{4}\left(\psi(1+\frac{y}{2}) + \psi(1-\frac{y}{2}) - \psi(1-x-\frac{y}{2}) - \psi(x+\frac{y}{2})\right) \\ E^{ICI}_{--_\perp}(x,y) &= E^{ICI}_{SI}(x+y), \end{aligned} \quad [S3]$$

and the $E^{ICI}_{\mu_\parallel}$ can be calculated in the same way as,

$$E^{ICI}_{\mu_\parallel}(x,y) = E^{ICI}_{++_\parallel}(x,y) + E^{ICI}_{+-_\parallel}(x,y) + E^{ICI}_{-+_\parallel}(x,y) + E^{ICI}_{--_\parallel}(x,y) \quad [S4]$$

where

$$\begin{aligned} E^{ICI}_{++_\parallel}(x,y) &= E^{ICI}_{--_\parallel}(x,y) = E^{ICI}_{SI}(x), \\ E^{ICI}_{+-_\parallel}(x,y) = E^{ICI}_{-+_\parallel}(x,y) &= \frac{q^2}{\epsilon L}\frac{1}{2}\left[\sum_{n=-\infty}^{\infty}\left(-\frac{1}{\sqrt{(2n-2x)^2+y^2}} - \frac{1}{\sqrt{(2n)^2+y^2}}\right) + \frac{1}{y}\right] \end{aligned} \quad [S5]$$

In Fig. S2, the two E^{ICI}_{μ} are calculated with $y = 1/40$ to mimic the aqueous electrolytes simulated in the main text; this is close to a O-H bond length with respect to the unit cell dimension $z \approx 4nm$. Noticeably, the ICI induced by the dipole is much shorter ranged compared to the ICI for single ion or symmetric ion pair. Another consequence of this is that the orientation of the dipole relative to the surface is not much affected by the ICI contribution of the energy until the dipole gets very close to the surface. When the dipole gets close enough to the surface, $E^{ICI}_{\mu_\parallel}$ can be twice more negative than $E^{ICI}_{\mu_\perp}$ at the same closest ion distance; for example, $E^{ICI}_{\mu_\parallel}(.1,.025) \approx -18.7652$, $E^{ICI}_{\mu_\perp}(.1,.025) \approx -9.921$.

Force field parameter utilized for all simulations

We have utilized the CHARMM Drude polarizable force fields (FFs)[2, 3] for polarizable simulations, and SPC/E water model[4] and corresponding ion FF[5] for non-polarizable simulations. The detailed FF parameters are given below. Note that the polarizable and non-polarizable models have very similar ion sizes (σ).

Atom	q	σ	ϵ	α
O	0.0	3.184	0.883	0.978
OM*	-1.11466	-	-	-
H	0.55733	-	-	-
Na	1.0	2.60	0.131	0.157
Cl	-1.0	4.42	0.301	3.969
I	-1.0	4.92	0.872	7.439

Table S1. Force field parameters used for polarizable simulations obtained from CHARMM Drude polarizable FFs.[2, 3] The units for σ, ϵ, and α are Å, kJ/mol, and Å^3, respectively. *The negative charge in CHARMM Drude water model is placed slightly off the oxygen atom (O), which is denoted as OM site.

[1] To whom correspondence should be addressed. E-mail: zgw@caltech.edu

Atom	q	σ	ϵ
O	-0.8476	3.166	0.650
H	0.4238	-	-
Na	1.0	2.59	0.42
Cl	-1.0	4.40	0.42
Br	-1.0	4.63	0.38
I	-1.0	5.17	0.42

Table S2. Force field parameters used for non-polarizable simulations obtained from SPC/E water model[4] and corresponding ion FF.[5] The units for σ and ϵ are Å and kJ/mol, respectively.

Simulations applying potential difference with constant surface charge

In Fig. S6, we show density profiles obtained from simulations with constant surface charge instead of constant electric field. We let each wall carbon atom on the two bounding surfaces carry charge of the same magnitude but opposite sign ($\pm q_0$; negative sign for the left electrode). To obtain q_0, we separate the total surface charge density (σ_{tot}) under external electric field into a static part (σ_0) and polarization part (σ_{pol}),[1, 6]

$$\begin{aligned}\sigma_{tot} &= \sigma_0 + \sigma_{pol} \\ &= \epsilon_0 \frac{\Delta V}{L} - \frac{1}{LA}\sum_i \langle z_i q_i \rangle\end{aligned} \quad [S6]$$

The second line defines σ_0 and σ_{pol}, where ΔV is the applied potential difference, A is the area of the electrode, and L is distance between the two bounding surfaces. σ_{pol} is the average of the instantaneous polarization of all the charges in the system, which is captured by ICPs. Thus only the static part of the surface charge ($\sigma_0 = \epsilon_0 \Delta V/L$) is used to set the explicit constant surface charge q_0,

$$\frac{q_0}{n^{WB}} = \frac{A\sigma_0}{N_C} = \frac{A\epsilon_0 \Delta V}{N_C L} = \frac{A\epsilon_0 E}{N_C} \quad [S7]$$

where N_C is the number of carbon atoms in each surface, ϵ_0 is the vacuum permittivity, $E = \Delta V/L$ is the applied electric field used in the constant-electric-field simulation. The scaling factor,

$$n^{WB} = \begin{cases} 2, & \text{for CW} \\ 1, & \text{for NPW} \end{cases} \quad [S8]$$

must be considered for CW boundary due to the use of 3D Ewald method with ICI; only half of the calculated 3D Ewald energy of the mirror-expanded system is accounted as the electrostatic force on the real particles.[1]

1. Hautman J, Halley JW, Rhee YJ (1989) Molecular dynamics simulation of water between two ideal classical metal walls. *J. Chem. Phys.* 91(1):467–472.
2. Lamoureux G, Harder E, Vorobyov IV, Roux B, MacKerell AD (2006) A polarizable model of water for molecular dynamics simulations of biomolecules. *Chem. Phys. Lett.* 418:245–249.
3. Yu H et al. (2010) Simulating monovalent and divalent ions in aqueous solution using a Drude polarizable force field. *J. Chem. Theory Comput.* 6:774–786.
4. Berendsen HJ, Grigera JR, Straatsma TP (1987) The missing term in effective pair potentials. *J. Phys. Chem.* 91(24):6269–6271.
5. Lee SH (1996) Molecular dynamics simulation of ion mobility. 2. alkali metal and halide ions using the spc/e model for water at 25 °c. *J. Phys. Chem.* 100(4):1420–1425.
6. Qing L, Zhao S, Wang ZG (2021) Surface charge density in electrical double layer capacitors with nanoscale cathode–anode separation. *J. Phys. Chem. B* 125(2):625–636.

Additional Information

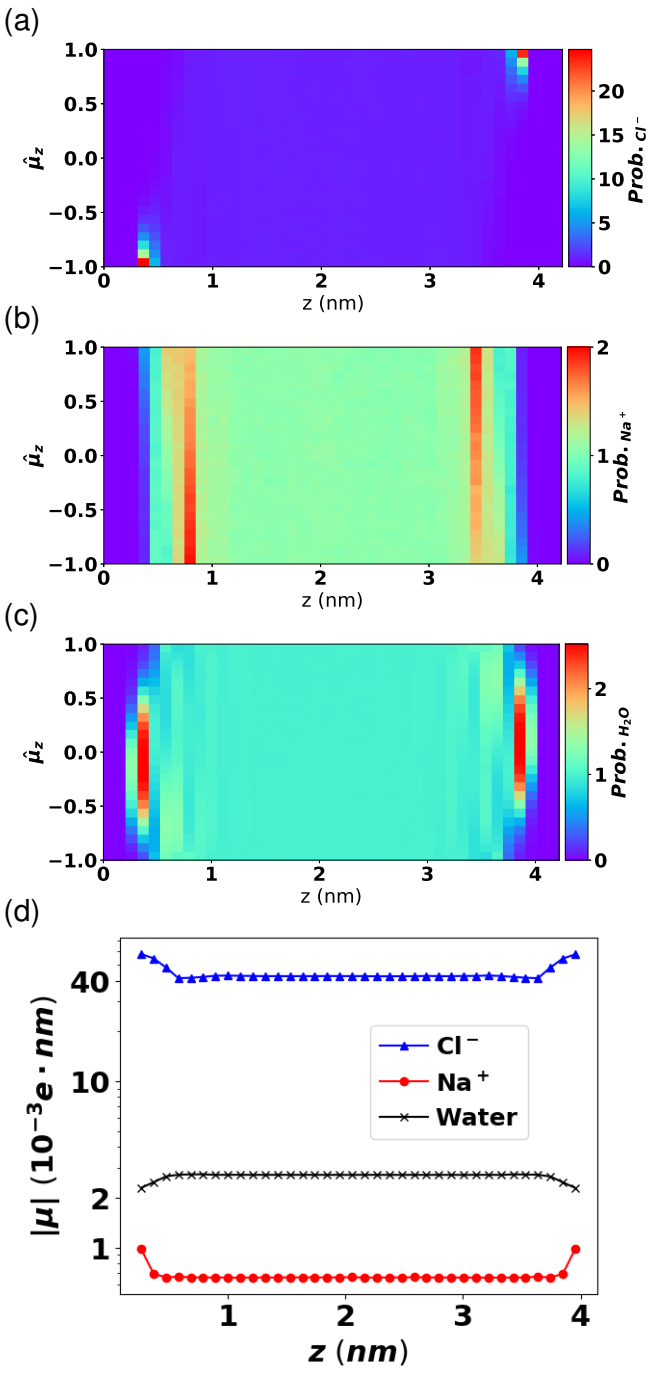

Fig. S3. Orientational probability distribution of the induced dipoles for (a) chloride ion, (b) sodium ion, and (c) water molecules simulated with polarizable FF. In all simulations, the surface is treated as fully polarizable surface (CW) and no external electric field is applied (0V). (d) The average magnitude of the induced dipole moment for each ions and water molecules at a distance z from the left surface. Near the surfaces, the magnitude of induced dipole increases for both of the ions while it decreases for water molecules. The chloride ions induces over 40 times larger dipole moment than sodium ions, which stabilizes the surface exposed ions.

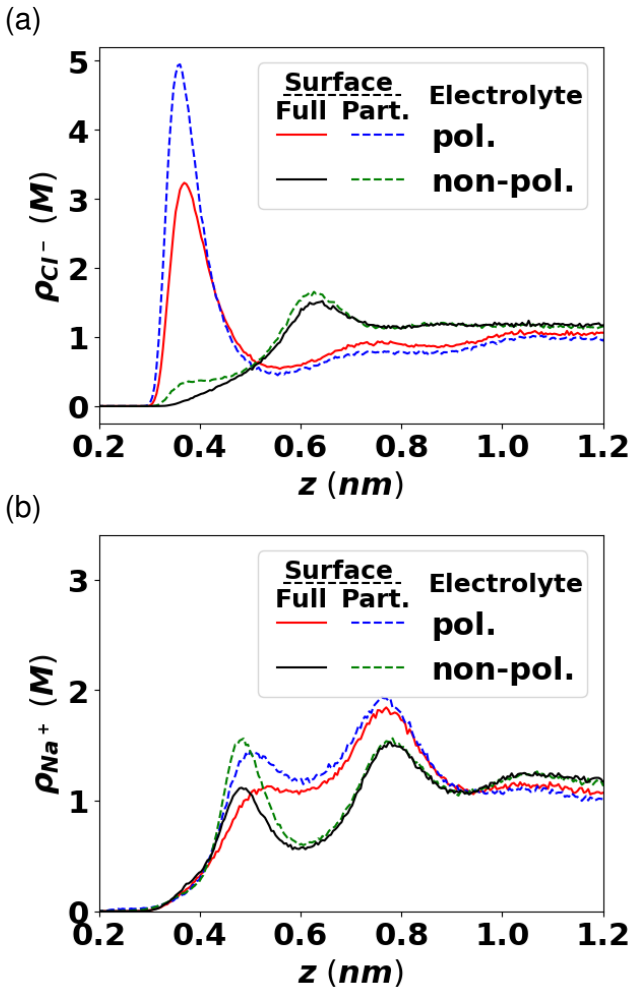

Fig. S4. Effect of partial ICI on the distribution of the (a) chloride and (b) sodium ions in 1M NaCl(aq) solution between two parallel plates under no applied electric field (0 V). The partial ICI (dashed lines) increases adsorption of both ions near the electrode compared to the results with full ICI (solid lines). For the simulation with non-polarizable FF and partial ICI, surface exposed chloride ion peak around z=0.4 nm is observed, which was not seen with full ICI. The screening of ion ICI by water ICI occurs regardless of the ion/solvent polarization; the ion distribution simulated with no ICI is almost identical to the distribution with full ICI for both polarizable FF and non-polarizable FF (Fig. 2 in the main text).

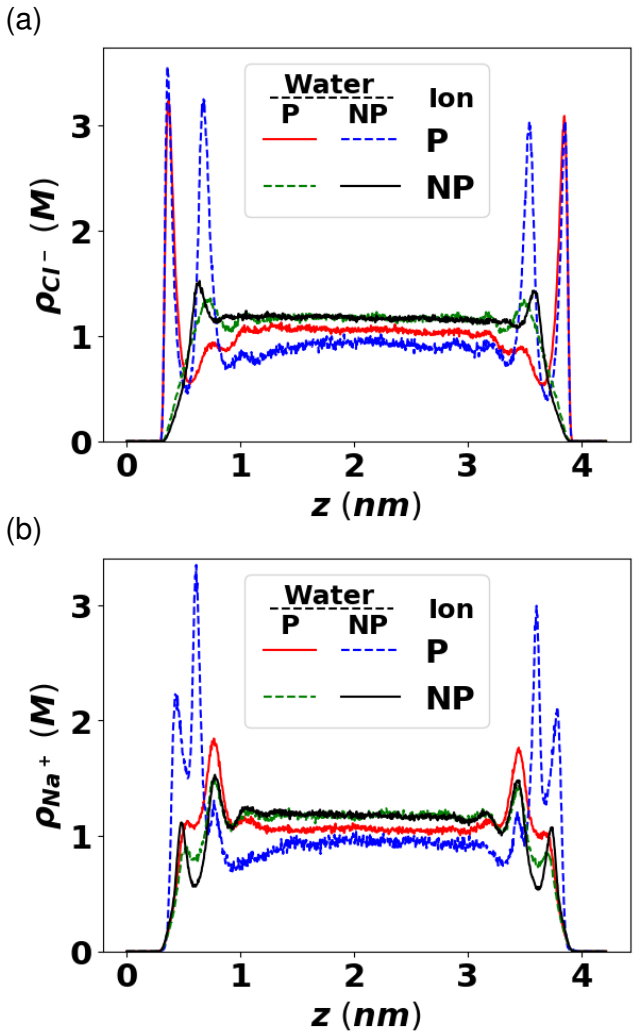

Fig. S5. Effect of partial ion/solvent molecular polarization models on the distribution of the (a) chloride and (b) sodium ions in 1M NaCl(aq) solution between two parallel plates under no applied electric field (0V). The surface is treated with full ICI representing graphene/water-like surface. In addition to the two sets of simulations in the main text Fig. 2 using polarizable (P, red solid lines) vs. non-polarizable (NP, black solid lines) FF for both water and ions, two sets of additional simulations are performed. In the first new simulation, the solvent polarizability is turned off from polarizable set (blue dashed lines). And in the second simulation, the ion polarizability is added to non-polarizable FF (green dashed lines). Surface-exposed chloride ion (peaks at z =0.4,3.8 nm) is only observed when ions are treated with polarizable FF.

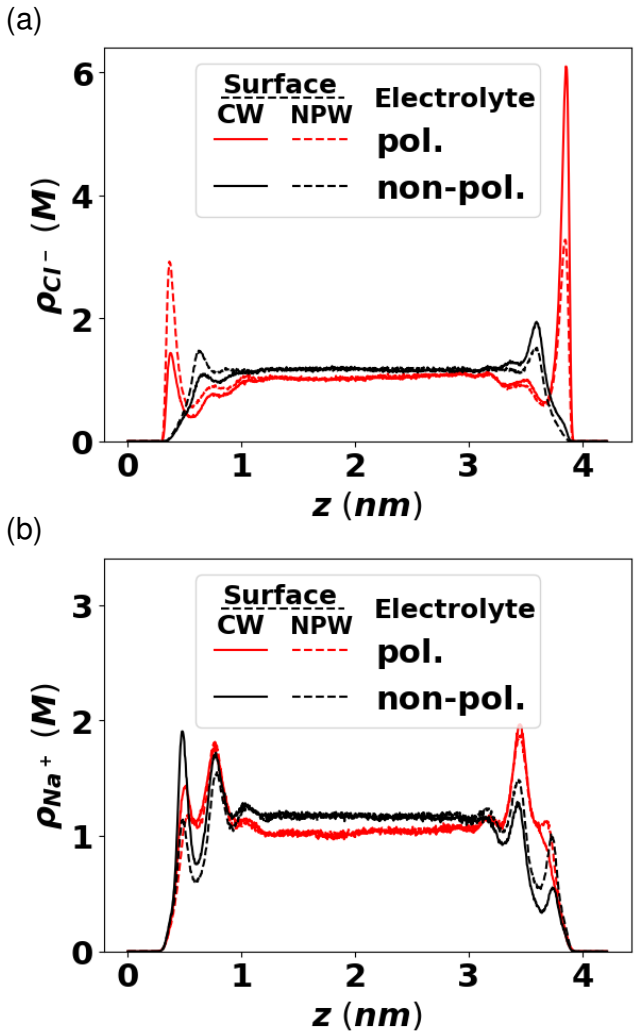

Fig. S6. Effect of ICl on the ion distribution of the (a) chloride and (b) sodium ions in 1M NaCl(aq) solution placed between two oppositely charged surfaces equivalent to 1V electrostatic potential difference (higher on the right surface) analogous to Fig. 4 in the main text. Each surface carbon atom carries static charge q_0 calculated by Eq. S7 ($q_0 = 6.8632 \times 10^{-4}$ for CW and $q_0 = 3.4316 \times 10^{-4}$ for NPW) to generate external electric field, while the surface polarization effect is modeled with ICPs. Consistent with Fig. 4 in main text, allowing surface polarization (CW, solid lines) significantly enhances charge separation under external electric field. The solid/dashed lines indicates CW/NPW surface, respectively, while the colors of the curves distinguishes polarizable/non-polarizable water and ion FF, analogous to Fig. 4 in the main text.

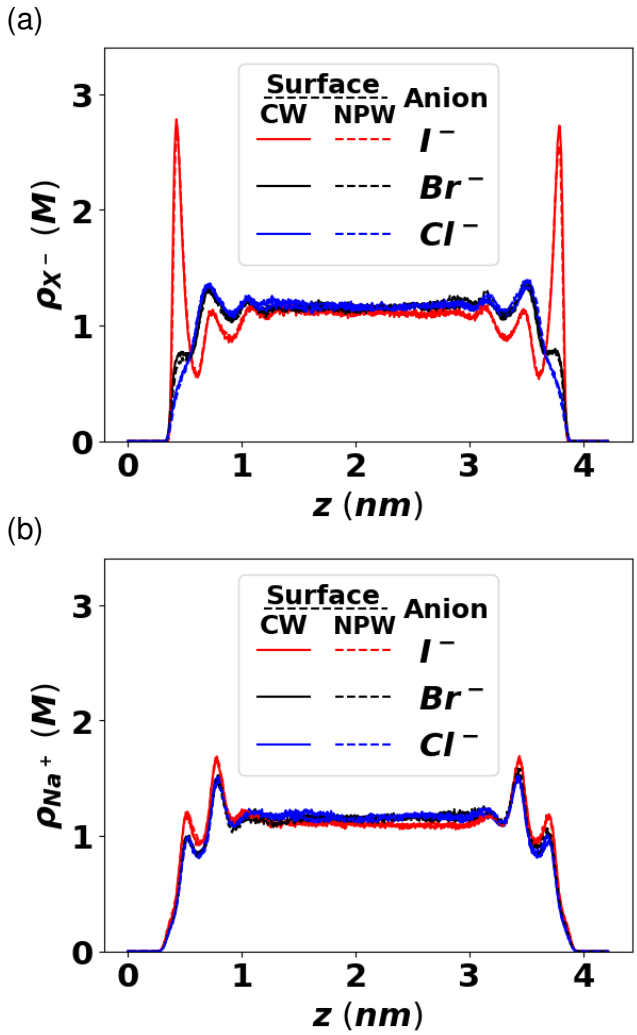

Fig. S7. Effect of varying anions and the surface polarization on the distribution of the (a) halide and (b) sodium ions in 1M NaX(aq) solution simulated with optimized non-polarizable FF. The electrolyte is confined between two parallel plates under no applied electric field (0V). The effect of ICl is almost completely screened by the ICl of solvent molecules; thus the density profiles for each ion are almost indistinguishable between the graphene-like surface with full ICl (CW, solid lines) or air/water like surface without any ICl (NPW, dashed lines). With the optimized non-polarizable FF, iodide ion concentration (red curves) shows strong surface enhancement, while bromide ion (black curves) has only minor exposure to the outermost layer and chloride ion (blue curves) is depleted from the surface.

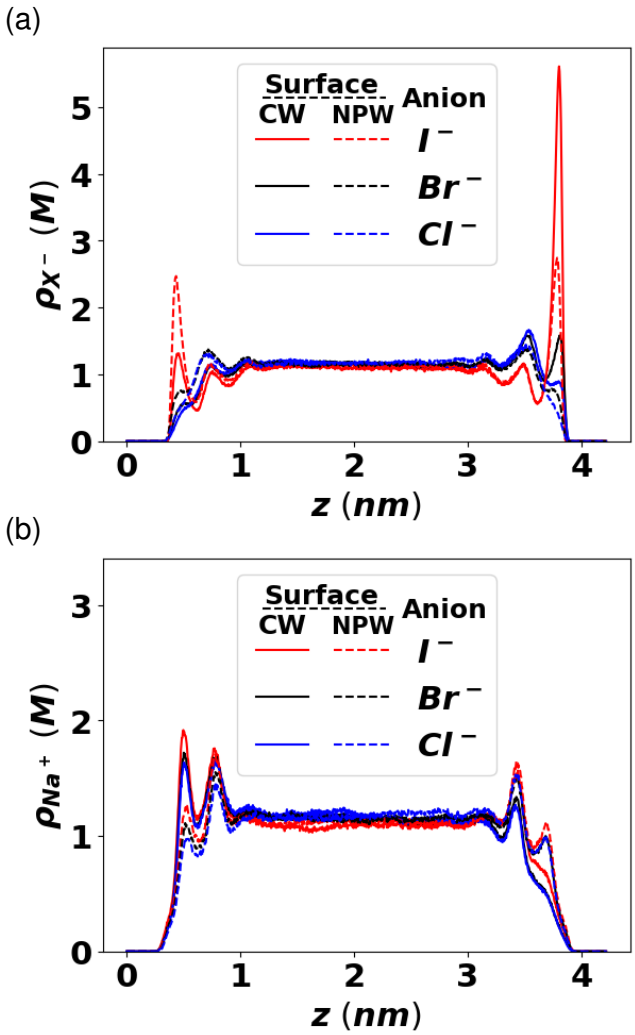

Fig. S8. Ion distribution of the (a) halide and (b) sodium ions in 1M NaX(aq) solution simulated with optimized non-polarizable FF under 1V external electric field. Analogous to Fig. 4(a),(b), allowing surface polarization (CW, solid lines) significantly enhances charge separation. The solid/dashed lines indicates CW/NPW surface, respectively, while the colors of the curves distinguishes polarizable/non-polarizable water and ion FF.

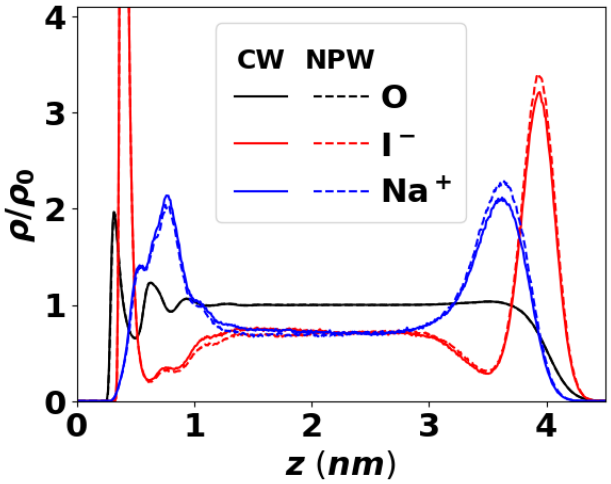

Fig. S9. Relative ion/water distribution in 1M NaI(aq) solution. The electrolyte with two boundary system is simulated with a polarizable FF and full ICI (CW) on the left hard graphene-like surface. A simulation without ICI (NPW) is also performed by not including any ICPs on the left side of the wall atoms. The right surface is allowed to freely fluctuate mimicking an air/water interface. Analogous to the main Fig. 6, allowing surface fluctuation on the right surface reduces the peak height and broadens the interfacial ion/water concentration peak, but the relative position of the surface species are consistent on both surfaces, showing both iodide and water molecules are exposed to both of the surfaces but sodium ions are solvent-separated (one water molecule apart) from the surfaces. Note the peak height for iodide at the air/water interface is much higher than that for chloride shown in Fig. 6 in the main text. Effect of ICI under zero external field is almost perfectly screened, resulting in two overlapping curves for each color.